Design and predicted performance of 4-m baseline Habitable-zone Exoplanet Observatory telescope

H. Philip Stahl,

NASA MARSHALL SPACE FLIGTH CENTER, HUNTSVILLE, AL 35812

ABSTRACT

The Habitable Exoplanet Observatory Mission (HabEx) is one of four missions which NASA is studying. Its goal is to directly image and spectroscopically characterize planets in the habitable zone around nearby sun-like stars. Additionally, HabEx would perform a broad range of general astrophysics science enabled by 115 to 1700 nm spectral range and 3x3 arc-minute FOV instruments. Critical to achieving its science goals is a large, ultra-stable UV/Optical/Near-IR (UVOIR) telescope. The baseline HabEx telescope is a 4-meter off-axis unobscured three-mirror-anastigmatic, diffraction limited at 400 nm with wavefront stability on the order of a few 10s of picometers. This paper summarizes how science driven systems engineering (using science requirements to derive engineering specifications) resulting in the opto-mechanical design of the HabEx baseline optical telescope assembly. And, how Structural Thermal Optical Performance (STOP) modeling predicts tolerance compliance.

Keywords: space telescopes, STOP Modeling

1. INTRODUCTION

The Habitable Exoplanet Observatory Mission (HabEx) has three goals: to seek out nearby worlds and explore their habitability; to map out nearby planetary systems and understand the diversity of the worlds they contain; and, to carry out observations that open up new windows on the universe from the UV through near-IR. **[1]** Using a science-driven systems-engineering method, the HabEx OTA design team derived specifications from science requirements (Table 1).

Table 1: HabEx Optical Telescope Specification flow-down from Science Requirements

Science	Telescope	Specification
Exoplanet: Inner Working Angle	Architecture	Off-Axis Unobscured Circular Aperture
	Aperture Diameter	> 3.7 meters
	Primary Mirror F/#	Slower than F/2.25 to minimize polarization cross-talk
	Diffraction Limit	400 nm
	Wavefront Error Stability	1 to 250 pm depending on coronagraph and spatial frequency
	Line of Sight Stability (Jitter)	< 0.3 milli-arc-seconds per axis
	Science Instruments	On the side (in the Secondary Mirror Tower structure) to maximize thermal stability and to minimize reflecting angles for polarization.
General Astrophysics: Wide FOV	Three-Mirror Anastigmatic	3 x 3 arc-min per instrument inside 21 arc-min diameter FOV
	Diffraction Limit	400 nm
UV Science	Spectral Range	115 nm to 1700 nm (nominal)
	Operating Temperature	270K (nominal); 260K (minimum)

Error budgets were created for each specification. Telescope point designs were created and evaluated for compliance with the error budget using STOP modeling. The point designs were then iterated and refined. **[2-5]**

Section 2 reviews how the HabEx Optical Telescope Assembly (OTA) specifications are derived from the HabEx science requirements. Section 3 describes the baseline opto-mechanical OTA design, its key components and design features. Section 4 summarizes detailed performance analysis of the baseline opto-mechanical design which shows that the design, using proven technology and engineering practice, can achieve the specifications necessary to perform HabEx science. Section 5 shows how STOP (structural thermal optical performance) model performance predictions are used to construct an error budget. The baseline 4-m off-axis HabEx opto-mechanical telescope design 'closes' for its line-of-sight (LOS) and wavefront error (WFE) stability specifications. The only external assumptions is that the mission is launched in an SLS 8.4-m fairing and uses low disturbance micro-thrusters for pointing control.

3. OTA SPECIFICATIONS

3.1 Aperture Architecture and Size

Exoplanet science drives the off-axis architecture, aperture diameter and primary mirror F/#. General astrophysics drives spectral range and requires a three mirror anastigmatic (TMA) design (Figure 1) to enable a wide field of view (FOV).

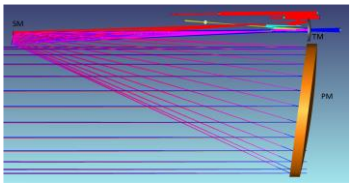

Figure 1: TMA Optical Design

Imaging habitable zone exoplanets using a coronagraph requires a telescope coronagraph 'system' that can produce a 10^{-10} 'dark hole' with as small of an inner working angle (IWA) as possible and as large of an irradiance throughput as possible. IWA is the minimum angular distance (on the sky) where the 'dark hole' begins – the location when the coronagraph can block 10^{10} of the host star's light (Figure 2). The smaller the IWA and the larger the throughput, the greater the number of habitable zones that can be searched. The ability to achieve a small IWA depends upon the telescope's ability to produce a small stable point spread function (PSF) with a compact stable encircled energy (EE). The smaller the EE, the smaller the IWA. It is common knowledge that the larger a telescope's aperture, the smaller its PSF and EE. But, what is often overlooked is that an unobscured (off-axis) telescope always has a more compact EE (better IWA) than an on-axis telescope with a central obscuration, because diffraction from the central obscuration broadens the PSF. To be specific, an unobscured circular aperture has 82.8% EE at λ/D. And, a telescope with a 10% central obscuration has 82.5% EE at 1.4 λ/D (and for a 20% obscuration, 82% EE is at 1.63 λ/D). **[7]** Additionally, diffraction from secondary mirror spider obscurations distort the PSF and broaden the EE. A 1 to 2% wide spider can increase EE diameter (IWA) by 5 to 10% **[7]** – requiring a 5 to 10% larger on-axis telescope. Of course the problem is even worse for a segmented aperture primary mirror.

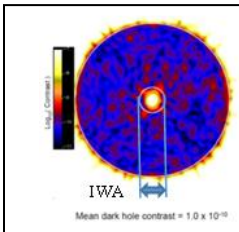

Figure 2: Dark Hole **[6]**

Throughput is the percent of the exoplanet's PSF core irradiance transmitted through the coronagraph as a function of angular separation between the host star and planet. Figure 3 shows the core throughput for three different coronagraphs – vector-vortex charge 4 (VVC4), charge 6 (VVC6) and hybrid Lyot (HLC) – all with the HabEx baseline 4-meter off-axis unobscured telescope; and, the throughput for a 6-m on-axis segmented primary mirror telescope (i.e. JWST) with an apodized pupil Lyot coronagraph (APLC). **[8-9]**

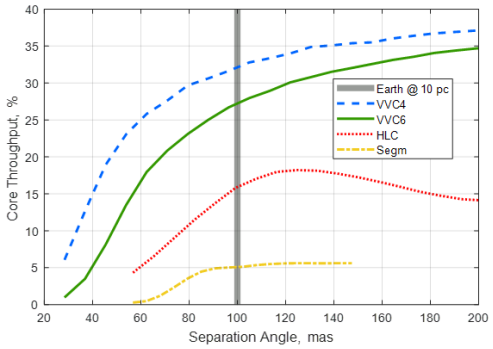

Figure 3: Core throughput versus separation angle. Vertical line is Exo-Earth at 10 pc (100 mas). **[8-9]**

Aperture and diffraction limit specifications are based on a design reference mission yield estimate for off-axis-telescope coronagraph combination. **[10]** Threshold science occurs when the telescope PSF core radius (λ/D) is < 25 mas. This is accomplished with a > 3.7-m off-axis monolithic telescope with a 400 nm diffraction limit.

To minimize polarization cross-talk in the coronagraph, a slow PM F/# is required. HabEx elected optical design similar to Exo-C with an F/2.5 primary mirror and the science instruments located on the anti-Sun side of the telescope. **[11]** Benefits of this configuration are that it minimizes the need for high angle of incidence reflections that produce unwanted polarization effects and isolates the coronagraph from thermal disturbances.

3.2 Diffraction Limited Performance

Diffraction Limit, along with aperture diameter, determines the performance parameters of PSF size, EE and Strehl ratio. A 400 nm diffraction limited telescope requires a system wavefront error (WFE) of approximately 30 nm rms. Contributors to telescope WFE are the primary mirror (PM), secondary mirror (SM) and tertiary mirror's (TM) surface figure errors, the ability to attached the PM and SM to the structure and accurately align them to the TM, and maintain that alignment on-orbit. Because the telescope has a laser metrology system to maintain alignment with high precision, the majority of the telescope's WFE budget can be allocated to the mirrors. And, because the PM is larger and less stiff, it gets the largest allocation. Figure 4 shows how the PM WFE engineering specification flows into an error budget

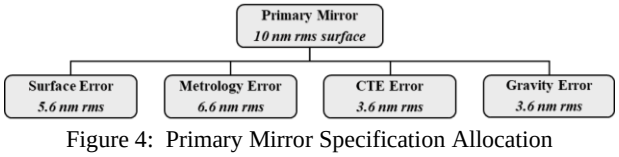

Figure 4: Primary Mirror Specification Allocation

which must be achieved by the PM fabrication process. Surface figure error allocation is set to what is demonstrated on WFIRST. Metrology error is set to what was demonstrated on JWST. The CTE error is set to the expected WFE produced by a mirror with ± 5 ppb/K CTE homogeneity manufactured at 300K and operating at 270K. **[12]** The gravity sag error is an allocation which requires technology development and demonstration.

General astrophysics and exoplanet science also drive the PM's spatial frequency specification. General astrophysics is most sensitive to the shape and stability of the PSF – which is driven by low-spatial frequency errors. And, exoplanet science is most sensitive to mid- and high-spatial frequency errors. Mid-spatial frequency errors blur or spread the core. And high-spatial frequency errors and surface roughness scatter light out of the core and over the entire PSF. Thus, per Table 2, the total PM surface figure specification is divided into low-, mid- and high-spatial frequency bands.

Table 2: Primary Mirror Error Specification

Total Surface Error	< 5.6 nm rms
Low Spatial SFE (< 30 cycles/dia)	< 4.3 nm rms
Mid Spatial SFE (30 to 100 cycles)	< 3.3 nm rms
High Spatial SFE (> 100 cycles)	< 1.4 nm rms
Roughness	< 0.3 nm rms

This specification assumes computer controlled polishing for spatial frequencies to 30 cycles (50 mm minimum tool size) to correct quilting error and a -2.5 PSD slope for high spatial frequencies. The 100-cycle boundary between mid and high spatial error is defined assuming that the coronagraph uses a 64 x 64 deformable mirror (DM). A 64×64 DM can theoretically correct spatial frequencies up to 32 cycles (or half the number of DM elements). This could create a 'dark hole' with an inner working angle (IWA) of λ/D and an outer working angle (OWA) of 32λ/D. The system engineering consideration is that primary mirror spatial frequency errors up to 3X beyond what can be corrected by the DM can scatter energy back into the 'dark hole'. Therefore, the primary mirror needs have a surface figure as smooth as possible for spatial frequency errors from 30 cycles up to 100 cycles. **[13-14]**

3.3 Line of Sight (LOS) Stability Specification

LOS instability is important for both general astrophysics and coronagraphy because it causes PSF smearing that degrades spatial resolution and IWA. A typical specification for LOS error is less than 1/10th the PSF radius. For a 400 nm diffraction limited 4-m telescope, the on-sky PSF radius is ~20 mas. Thus, the specification should be < 2 mas. But, the coronagraph requires a LOS stability better than 0.3 mas per axis. The reason is that LOS error causes beam-shear on the SM and TM, as well as other mirrors in the optical train, which introduces dynamic WFE that result in contrast leakage.

Two sources of LOS instability are thermal and mechanical. LOS thermal drift occurs when the telescope is slewed relative to the Sun. Fortunately, this effect is slow and can be corrected. HabEx is baselining a laser-truss system to sense and correct slow LOS drift. LOS jitter is more important. Jitter is produced by mechanical disturbance accelerations (from sources such as reaction wheels, cryo-coolers, etc.) exciting modes in the telescope structure. To correct 'slow' jitter (i.e. < 10 Hz), HabEx is baselining a low-order Wavefront Sensor similar to the WFIRST system that can sense and correct LOS jitter on the order of 2.5 mas to less than 0.3 mas per axis. But, given that the sensor does not correct jitter at frequencies above 10 Hz, the telescope is specified to meet the uncorrectable jitter specification of 0.3 mas per axis.

To design the telescope, it is necessary to convert the LOS stability specification into an engineering tolerance, i.e. maximum allowed optical component rigid body motions. Zemax tolerance analysis of the baseline optical design provides the LOS and WFE sensitivity to rigid body motions of the primary and secondary mirrors relative to the tertiary mirror for the baseline F/2.5 optical design **[3]**. From these sensitivities, an LOS error budget can be allocated for each rigid body degree of freedom (DOF) to keep the on-sky LOS jitter < 0.3 mas per axis specification. Figure 5 shows one potential error budget allocation.

Specification				0.3	mas
				ALLOCATION (one sided P	
Alignment	ZEMAX	Tolerance	units	RSS	Units
PM X-Decent	DX	2	nanometer	0.043	mas
PM Y-Decent	DY	2	nanometer	0.042	mas
PM Z-Despac	DZ	1	nanometer	0.005	mas
PM Y-Tilt	TX	0.5	nano-radian	0.204	mas
PM X-Tilt	TY	0.5	nano-radian	0.200	mas
PM Z-Rotatic	TZ	0.5	nano-radian	0.027	mas
SM X-Decent	DX	2	nanometer	0.038	mas
SM Y-Decent	DY	2	nanometer	0.037	mas
SM Z-Despac	DZ	1	nanometer	0.005	mas
SM Y-Tilt	TX	0.5	nano-radian	0.019	mas
SM X-Tilt	TY	0.5	nano-radian	0.019	mas
SM Z-Rotatic	TZ	0.5	nano-radian	0.002	mas
RSS LOS Error				0.3	mas

Figure 5: Rigid body motion tolerance allocation to meet < 0.3 mas uncorrectable LOS Stability specification.

3.4 Wavefront Error (WFE) Stability Specification

WFE stability specification is driven by the coronagraph. Any temporal or dynamic change in WFE can result in dark-hole speckles that produce a false exoplanet measurement or mask a true signal. The required WFE stability error budget is based on the total allowable coronagraph contrast leakage which enables the detection, at a defined signal to noise ratio,

of an exoplanet with a given flux ratio relative to its host star by a coronagraph with specific noise properties. **[8-9]** For the case of an exo-Earth at 10 parsecs, the planet is detectable as long as WFE instability produces < 40 ppt of contrast leakage. To be conservative, the HabEx study assumed 30 ppt. The next step is to calculate the coronagraph's contrast leakage for each Zernike polynomial. Then, using this sensitivity, allocate the 30 ppt on an RSS basis between each Zernike term to produce an error budget tolerance specification.

Figure 6 shows this process for the Vector Vortex Charge-6 Coronagraph (VVC-6). The first data column shows the contrast leakage sensitivity to each Zernike term. The VVC-6 is insensitive to lower order error up to spherical and very sensitive to trefoil and higher errors. The next column shows a completely arbitrary RSS allocation of 30 ppt of contrast. Multiplying these allocations by the sensitivity yields an initial wavefront error budget. But, these errors must be sub-allocated to the actual physical mechanisms by which they arise: LOS Jitter, Inertial Deformation and Thermal. For purposes of initial analysis, we did a simple uniform allocation.

		Allocation			100%	33%	33%	33%
				30				
Index			VVC-6 Sensitivity	Contrast Allocation	VVC-6 Tolerance	LOS	Inertial	Thermal
N	M	Aberration	[ppt/pm]	[ppt]	[pm rms]	[pm rms]	[pm rms]	[pm rms]
		TOTAL RMS		30.00	4381.1	2528	2528	2528
1	1	Tilt	2.13E-04	1.00	2342.6	1351.83	1351.83	1351.83
2	0	Power (Defocus)	3.30E-04	1.00	1751.9	1010.98	1010.98	1010.98
2	2	Astigmatism	1.92E-04	1.00	2121.2	1224.08	1224.08	1224.08
3	1	Coma	1.87E-04	1.00	1888.2	1089.60	1089.60	1089.60
4	0	Spherical	2.79E-04	1.00	1603.7	925.42	925.42	925.42
3	3	Trefoil	1.00	8.00	2.8	1.63	1.63	1.63
4	2	Sec Astigmatism	1.650	8.00	1.5	0.88	0.88	0.88
5	1	Sec Coma	1.665	8.00	1.4	0.80	0.80	0.80
6	0	Sec Spherical	2.890	8.00	1.0	0.60	0.60	0.60
4	4	Tetrafoil	0.931	8.00	2.7	1.57	1.57	1.57
5	3	Sec Trefoil	1.820	8.00	1.3	0.73	0.73	0.73
6	2	Ter Astigmatism	2.722	8.00	0.8	0.45	0.45	0.45
7	1	Ter Coma	3.061	8.00	0.7	0.38	0.38	0.38
5	5	Pentafoil	2.441	8.00	0.9	0.55	0.55	0.55
6	4	Sec Tetrafoil	2.205	8.00	1.0	0.56	0.56	0.56
7	3	Ter Trefoil	2.795	8.00	0.7	0.41	0.41	0.41
6	6	Hexafoil	3.167	8.00	0.7	0.39	0.39	0.39
7	5	Sec Pentafoil	3.069	8.00	0.7	0.38	0.38	0.38
7	7	Septafoil	2.651	8.00	0.8	0.44	0.44	0.44

Figure 6: Allocation of WFE Stability between LOS, Inertial and Thermal Sources.

LOS WFE instability occurs when LOS jitter or drift causes beam-shear on the secondary and tertiary mirrors. Because they are conics, beam shear manifests itself as low-order astigmatism and coma (shear of spherical aberration is coma and sub-aperture coma appears to be astigmatism). Inertial WFE instability occurs when the primary mirror is accelerated, by mechanical disturbances, causing it to react (i.e. bend) against its mounts. The shape of this error is similar to the mirror's static (X,Y,Z) gravity sag (i.e. bending of the mirror when it is exposed to a 1G acceleration in the X,Y,Z directions). Therefore, the shape of the inertial instability can be tailored by adjusting the geometry of the mirror mount design, i.e. 3 vs 6 vs 9-point mount, and location of mounts, i.e. edge vs 70% radius.

Thermal WFE instability occurs when the primary mirror's bulk temperature or temperature gradient changes. If the mirror's coefficient of thermal expansion (CTE) is completely homogeneous and constant, then a bulk temperature should only result is a defocus error. But any inhomogeneity in the mirror's CTE will result in a temperature dependent WFE. Additionally, because CTE is itself temperature dependent, any change in the mirror's thermal gradient will also result in a WFE. Unlike mechanical WFE which is mostly low-spatial-frequency, thermal WFE can have significant high-spatial-frequency content. Therefore, the best mitigation strategy is to minimize thermal disturbances. This can be done either by passive isolation or active sense and control.

4. OPTO-MECHANICAL DESIGN

The 'baseline' telescope (Figure 7) consists of the PMA, SMA, SM tower with integrated science instrument module, and stray-light tube with 40-deg forward scarf. The tower and baffle tube are the optical bench which maintains alignment between the PMA, SMA and TMA. The OTA is physically separate from the spacecraft which includes the solar array sunshield. The size of the solar arrays on the bottom are driven by thermal power requirements during anti-sun pointing. Instead of reaction wheels, thrusters are used for slewing the observatory and micro-thrusters are used for fine pointing control during science observations. The OTA and spacecraft connect only at the interface ring. This ring is also the interface between the payload and the Space Launch System (SLS).

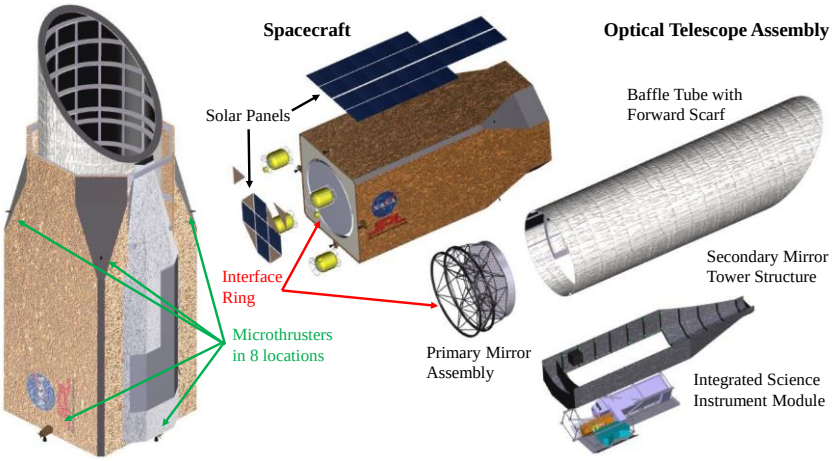

Figure 7: Baseline HabEx Observatory Payload

The Baseline Observatory is designed for the SLS Block 1B mass and volume capacities, and launch environment. **[15]** The payload fits inside the SLS 8.4-m fairing with no deployments. The projected total mass (with 30% reserve) of 14-mt has significant margin against the SLS Block-2 capacity of 44 mt to SE-L2. The telescope and spacecraft structure are designed to have a first mode higher than 10 Hz and to survive a 3.5g axial and 1.5g lateral launch load.

The structure is the foundation for the entire telescope. It is the optical bench to which the optical components and science instruments are attached. It has the critical function of placing the primary, secondary and tertiary mirrors at the locations specified by the optical design and keeping them at those locations with sufficient stability to meet the required performance specifications. This is accomplished by making the structure as stiff as possible and by minimizing the disturbances to which the structure is exposed. Given that the optical design is a TMA and that three of the four science instruments share a common tertiary mirror. The TM location is fixed, and the primary and secondary mirror alignments are adjusted relative to the TM. STOP modeling predicts that the baseline structure meets the LOS Jitter and LOS WFE stability specification for a specified micro-thruster disturbance profile.

The HabEx design team conducted multiple trade studies to optimize the stiffness, mass and gravity sag of candidate open-back Zerodur® and closed-back ULE® primary mirrors. Design parameters traded included facesheet thickness, mirror thickness, core wall thickness, core pocket size, core geometry, and mount geometry (i.e. edge mount R = 100% vs R = 80% or 67%). **[16-20]** Zerodur® was selected as the baseline material because Schott has demonstrated a routine ability to fabricate 4.2-m diameter Zerodur® substrates and turn them into lightweight structures via their extreme-lightweight Zerodur® Mirror (ELZM) machining process. And, because a 1.2-m Zerodur® ELZM mirror owned by Schott and tested at NASA MSFC showed better thermal stability than a 1.5-m ULE® mirror manufactured as part of the AMTD project. **[21]** Part of Zerodur's CTE advantage over ULE is that the mirror is fabricated from a single boule of material, thus a Zerodur® mirror has a more homogeneous CTE distribution than a mirror assembled from multiple ULE® components.

The baseline Zerodur® mirror assembly provides an excellent balance between mass and stiffness. The substrate has a flat-back geometry with a 42 cm edge thickness and mass of approximately 1400 kg. The mirror's free-free first mode frequency is 88 Hz. And, its mounted first mode frequency is 70 Hz. Mass is important because it provides thermal capacity for a thermally stable mirror. Additionally, mass allows for local stiffening of the substrate to minimize gravity sag. **[16]** The mirror substrate geometry and hexapod mount designs were optimized to produce as uniform as possible XYZ gravity sag deformation. The mirror is attached at three edge locations to a hexapod mount system. This geometry was selected to allow defocus and minimize spherical gravity sag based on vector vortex coronagraph aberration sensitive.

The primary mirror thermal control system is critical to the telescope's ability to achieve science required diffraction limited performance and wavefront stability. It sets the primary mirror's front surface to the desired operating temperature and keeps it at that temperature regardless of where the telescope points on the sky relative to the sun. Control system accuracy impacts diffraction limit performance, signal to noise and spectral throughput. And, the precision to which the system can maintain temperature determines wavefront stability. Any gradient or bias error in the mirror's bulk temperature will introduce a static 'cryo-deformation' wavefront error. And, any temporal variation in the mirror's temperature will introduce instability.

Similar to Hubble, HabEx cold biases the primary and secondary mirrors and heats them to their operating temperature. The operating temperature is constrained by two competing requirements. Near-IR science requires cold mirrors to minimize in-field thermal noise. But, UV science requires the mirrors to be free of any contamination such as a monolayer of water ice or other out-gassed molecules to maximize spectral throughput. HabEx has selected an operating temperature of 270K for its mirrors because it is above the sublimation temperature for water ice. The amount of cold bias is also constrained by competing engineering requirements. The greater the bias, the easier it is to control the mirror temperature; but the more electrical power required to achieve that control. The minimum amount is one where the mirrors are cold biased for all potential sun orientation angles. Cold bias is produced by thermal isolation around the telescope.

HabEx plans to use a thermal control system with radial and azimuthal heater zones behind and around the primary mirror. The radial heater zones compensate for the view factor radial gradient to create a uniform front surface temperature. And, the azimuthal heater zones compensate for changes in the lateral thermal gradient as a function of pointing angle.

The baseline HabEx active radial thermal control concept is an engineering scale-up of systems built by the Harris Corporation. Zonal active thermal control of primary mirrors is currently TRL-9 with systems currently flying on the Harris Corporation commercial 0.7-m and 1.1-m Spaceview™ telescopes. These systems enable on-orbit focus adjustment for optimal image quality. **[22, 23]** Additionally, under the Astrophysics Division funded Predictive Thermal Control Study (PTCS), Harris Corporation has built and delivered to NASA, for testing with candidate mirror assemblies, a 1.5-m system with 25 thermal control zones (Figure 8). **[24]** This system has 6 azimuthal heater zones in each of 4 radial and circumferential zones. Additionally, there are heater zones on each mirror strut and the support structure. The test article is fully instrumented to quantify radiative and conductive heat flow.

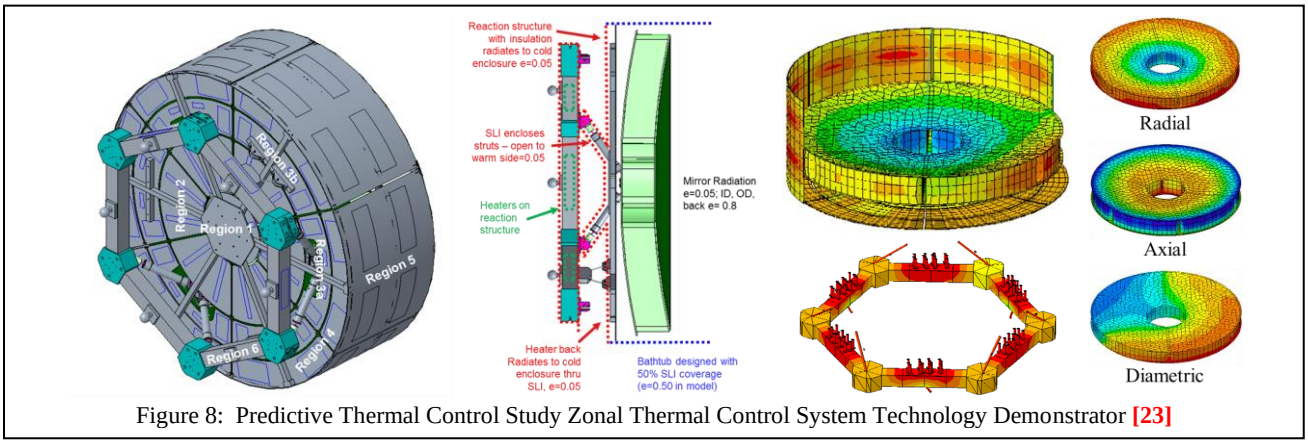

Figure 8: Predictive Thermal Control Study Zonal Thermal Control System Technology Demonstrator **[23]**

5. STOP MODEL ANALYSIS

5.1 Integrated Model

To evaluate if the baseline HabEx telescope meets its performance requirements, integrated thermal and finite element models (FEM) were constructed of the telescope and spacecraft bus then merged into an observatory model. An observatory model is required because the telescope's thermal and mechanical performance is strongly influenced by the spacecraft. These models were used to perform structural thermal opto-mechanical performance (STOP) analyses. The observatory FEM was created using the MSC Patran pre-processor and geometry created in Pro-Engineer CAD. The primary and secondary mirror FEMs were created independently using the NASA MSFC Arnold Mirror Modeler. An integrated NASTRAN model, analyses was performed to ensure strength/stability and stiffness requirements were satisfied in accordance with NASA-STD5001B and the launch vehicle payload users guide (ULA - Delta IV Heavy). Additionally, the integrated FEM was used to perform dynamic response, and thermal analysis. The observatory thermal model was created in Thermal Desktop using the geometry created in Pro-Engineer CAD. The Thermal Desktop model has 20K elements and calculates telescope's structure and mirror temperature distribution at 10K nodes. The temperature distribution for each node is mapped onto the NASTRAN FEM and the deflections created by each node's coefficient of expansion (CTE) is calculated using NASTRAN Solution 101. Rigid body motions (RBM) and mirror surface deformations are calculated from the NASTRAN deflections using SigFit. The primary and secondary mirror's mesh grids were sized to enable SigFit to fit thermally induced surface figure error (SFE) to higher order Zernike polynomials.

Dynamic mechanical errors (LOS jitter, LOS WFE stability, inertial WFE stability, and impulse ring-down) are caused by structural response to mechanical stimuli. To minimize the source of such stimuli, the baseline HabEx observatory architecture does not use reaction wheels for slewing and pointing. Instead it uses thrusters and micro-thrusters. Thursters slew and point the telescope. During science exposures, they are turned off and micro-thrusters maintain pointing. Thus, micro-thruster noise is the only source of mechanical stimuli. Micro-thrusters run continuously with thrust proportional to applied current, Figure 9 shows a measured noise PSD for a single colloidal micro-thruster emitter. The data indicates that micro-thrusters have a maximum noise of about 0.03 μN/√Hz with a roll-off after about 2 Hz. **[25]** But, because the data is noisy and has not been measured beyond 5 Hz, the HabEx STOP analysis assumed that each micro-thruster emitter has a flat or 'white' noise spectrum of 0.1 micro-Newton – providing a 5X model uncertainty factor. Because the aft modules have twice as many emitter heads as the forward modules, each forward module is specified to have a flat noise spectrum of 0.4 μN/√Hz and each aft module is specified to have 0.8 μN/√Hz.

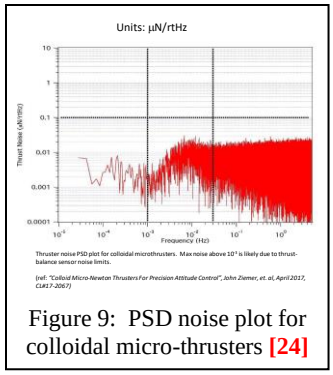

Figure 9: PSD noise plot for colloidal micro-thrusters **[24]**

Dynamic thermal errors (LOS drift, LOS WFE, and thermal WFE stability) are caused by structural and optical component response to thermal stimuli. To predict thermal performance, a 250 hour design reference mission (DRMs) was analyzed in Thermal Desktop. The calculated temperature distribution is mapped onto the NASTRAN FEM and the deflections of each node calculated. Rigid body motions and surface figure errors (SFE) of the primary and secondary mirrors were calculated from the NASTRAN deflections using SigFit.

The DRM starts by pointing the telescope at a reference star to dig the dark hole. The analysis assumes that the telescope reaches a steady state thermal condition at this sun orientation. Next, the telescope is pointed at the science star. To make the analysis worst-case, it is assumed that this requires a +θ degree pitch away from the sun. To facilitate speckle subtraction, the telescope is rolled ± Φ degrees about the science star vector.

5.2 Predicted LOS Stability Performance

Mechanical LOS stability performance, the rigid-body motion of the primary and secondary mirrors relative to the tertiary mirror were calculated as a result of the structure's response from 0 to 350 Hz to the micro-thruster noise specification applied to the structure from 0 to 10 Hz (Figure 9). The specification provides at least a 2X margin at low frequencies and more margin at higher frequencies. Additionally, a MUF of 2 was applied for a total margin of ~4X. Typically the results of this analysis would be presented as a plot of displacement vs frequency because all previous space telescopes used reaction wheels which operate over a range of frequencies. But, HabEx is using microthrusters which are always on and simultaneously excite the structure over the entire frequency range. Therefore, it is necessary to take an extra step and RSS the individual components into a running sum. Figures 10 and 11 shows the cumulative rigid body displacement and rotations for the primary and secondary mirrors.

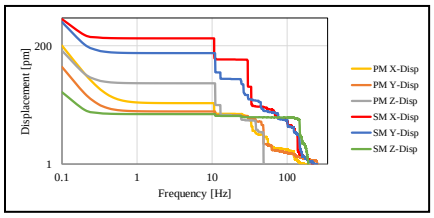

Figure 10: Cumulative Primary and Secondary mirror rigid body displacement for micro-thruster noise specification

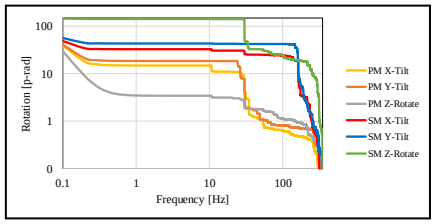

Figure 11: Cumulative Primary and Secondary mirror rigid body displacement for micro-thruster noise specification

Table 3 lists the maximum amplitude for each rigid body motion (with MUFs). Collectively, these motions predict an LOS jitter of ~0.03 mas which provides a ~10X performance margin against the 0.3 mas (> 10 Hz) specification.

Table 3: Max motion of PM and SM from Microthruster Noise

DOF	Δx (nm)	Δy (nm)	Δz (nm)	Θx (nrad)	Θy (nrad)	Θz (nrad)
Primary	0.20	0.08	0.16	0.04	0.04	0.03
Secondary	0.67	0.58	0.03	0.05	0.06	0.15

To predict thermal LOS stability performance, the rigid-body motions of each mirror was calculated for the 250-hr DRM. Figures 12 and 13 show the XYZ rigid body residual displacements of the primary and secondary mirrors, i.e. the amount of thermal rigid body motion that is not corrected by the laser metrology system that senses and controls the optical alignment of the primary and secondary mirrors.

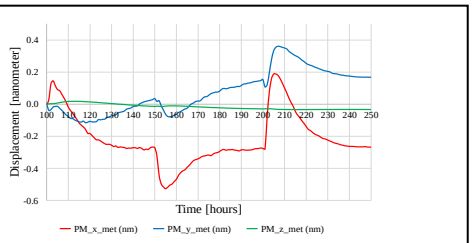

Figure 12: Displacements of PM due to thermal DRM

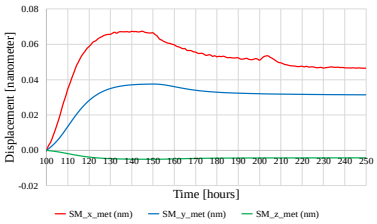

Figure 13: Displacements of SM due to thermal DRM

Taking the maximum uncorrectable motion for each rigid-body degree of freedom of the primary and secondary mirrors predict an LOS thermal drift of less than 0.2 mas (i.e. ~12.5X margin) against the 2.5 mas (< 10 Hz) specification. In this case, no MUF is applied.

5.3 Predicted WFE Stability Performance

Predicted WFE Stability from LOS Jitter as a function of Zernike polynomial is calculated from the predicted PM and SM motions. As expected, the largest LOS errors are tilt, power and astigmatism. But these errors are not significant to the VVC-6. The most significant are trefoil and secondary astigmatism. But, because the LOS jitter is so small, the predicted amplitudes for these errors have >100X margin relative to their error budget allocation (Figure 14)

Inertial WFE instability occurs when the PM is accelerated by mechanical disturbances causing it to react (i.e. bend) against its mounts. Figure 15 illustrate how the mirror bends as it reacts against the hexapod mount for the rocking and bouncing modes.

Index			Allocation LOS		LOS RSS WFE
N	M	Aberration	[pm rms]	MARGIN	(pm rms)
		TOTAL RMS	2528	1430	1.767
1	1	Tilt	1351.83	1984	0.681
2	0	Power (Defocus)	1010.98	837	1.208
2	2	Astigmatism	1224.08	1145	1.069
3	1	Coma	1089.60	4547	0.240
4	0	Spherical	925.42	212904	0.004
3	3	Trefoil	1.63	141	0.012
4	2	Sec Astigmatism	0.88	201	0.004
5	1	Sec Coma	0.80	1179	0.001
6	0	Sec Spherical	0.60	42835	0.000
4	4	Tetrafoil	1.57	11780	0.000
5	3	Sec Trefoil	0.73	12189	0.000
6	2	Ter Astigmatism	0.45	29360	0.000
7	1	Ter Coma	0.38	229124	0.000
5	5	Pri Pentafoil	0.55	356736	0.000
6	4	Sec Tetrafoil	0.56	740369	0.000
7	3	Ter Trefoil	0.41	1376489	0.000
6	6	Hexafoil	0.39	3944935	0.000
7	5	Sec Pentafoil	0.38	4982996	0.000
7	7	Pri Septafoil	0.44	6511622	0.000

Figure 14: LOS WFE stability predicted to have >100X margin relative to error budget allocation.

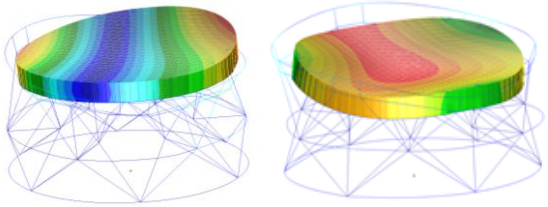
Figure 15: Mirror bending from (left) 49.5 Hz Rocking Mode; (right) 50 Hz Bouncing Mode

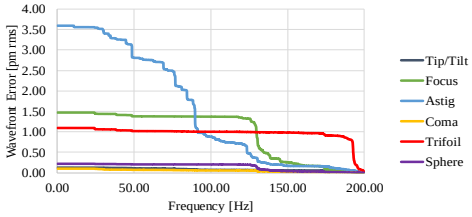

Figure 16: Total PM Inertial Deformation of select Zernikes: Astig = 3.6 pm rms; Focus = 1.5 pm rms; Trefoil = 1.1 pm rms

NASTRAN calculated the displacement of PM surface nodes from 0 to 350 Hz as a function of the micro-thruster noise specification applied to the structure from 0 to 10 HZ. To eliminate rigid body displacements, the node displacements were calculated relative to a fixed surface reference point. The WFE produced by these displacements were fit to Zernike polynomials using SigFig. And, because the microthrusters excite all modes simultaneously, the individual frequencies were RSSed to yield a total accumulated WFE for each Zernike term (Figure 16).

Consistent with mass dampening (i.e. where the mirror has a smaller response to higher frequency accelerations), the non-linear analysis predicts an astigmatism WFE that is 3X smaller, a focus error that is 4X smaller, and a trefoil WFE that is 5X smaller than the simple linear gravity sag scaling approach. Figure 17 shows how the calculated inertial WFE of the primary mirror compares with its simple error budget allocation. As expected Trefoil is the dominant term, but still has 1.6X margin.

			Inertial WFE Stability		
			Allocation		Zernikes
Index			Inertial	MARGIN	[pm rms]
N	M	Aberration	[pm rms]		
		TOTAL RMS	891.94		3.994
1	1	Tilt	1351.83	10990.5	0.123
2	0	Power (Defocus)	1010.98	707.0	1.430
2	2	Astigmatism	1224.08	343.9	3.559
3	1	Coma	1089.60	11006.1	0.099
4	0	Spherical	925.42	4344.7	0.213
3	3	Trefoil	1.63	1.6	1.039
4	2	Sec Astigmatism	0.88	5.0	0.178
5	1	Sec Coma	0.80	30.8	0.026
6	0	Sec Spherical	0.60	21.5	0.028
4	4	Tetrafoil	1.57	7.9	0.198
5	3	Sec Trefoil	0.73	6.5	0.112
6	2	Ter Astigmatism	0.45	21.6	0.021
7	1	Ter Coma	0.38	11.4	0.033
5	5	Pentafoil	0.55	7.4	0.074
6	4	Sec Tetrafoil	0.56	19.3	0.029
7	3	Ter Trefoil	0.41	27.5	0.015
6	6	Hexafoil	0.39	15.0	0.026
7	5	Sec Pentafoil	0.38	25.1	0.015
7	7	Septafoil	0.44	43.5	0.010

Figure 17: Estimated Inertial Wavefront Error.

Thermal WFE instability was predicted by applying the 250 hr DRM to the integrated model. Thermal Desktop calculated the temperature distribution as a function of time. With this distribution, NASTRAN calculated surface deformations which were then used by SigFit to decompose the temporal WFE into Zernike polynomials as a function of time. Figure 18 shows the predicted change in primary mirror surface figure error decomposed into Zernike polynomials. As symmetric errors, power and trefoil's changes are caused by the DRM pitch angle, which changes the total solar load on the telescope. And as an asymmetric error, astigmatism's change is caused by the DRM roll which shifts thermal load from one side to the other.

Total DRM wavefront error was calculated by RSSing the PM and SM Zernike terms as a function of time and selecting the maximum amplitude for each. This analysis has a 3X MUF. Figure 19 shows each Zernike compared to the simple error budget. Obviously, trefoil is a problem. Fortunately there is a solution. Reallocate the error budget.

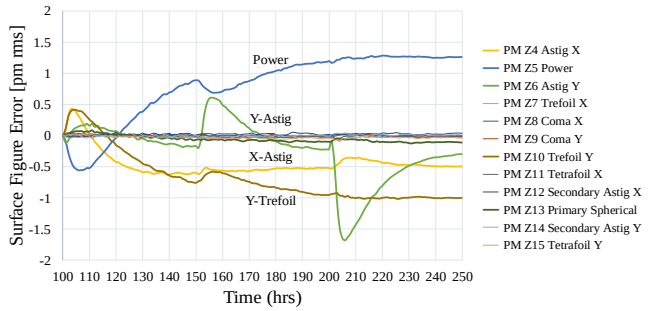

Figure 18: DRM primary mirror SFE changes

			Thermal WFE Stability		
			Allocation		Zernike
Index			Thermal	MARGIN	[pm rms]
N	M	Aberration	[pm rms]		
		TOTAL RMS	2528.15		5.565
1	1	Tilt	1351.83	51993.3	0.026
2	0	Power (Defocus)	1010.98	268.9	3.759
2	2	Astigmatism	1224.08	353.5	3.463
3	1	Coma	1089.60	3158.3	0.345
4	0	Spherical	925.42	2285.0	0.405
3	3	Trefoil	1.63	0.8	2.098
4	2	Sec Astigmatism	0.88	8.2	0.108
5	1	Sec Coma	0.80	7.6	0.105
6	0	Sec Spherical	0.60		
4	4	Tetrafoil	1.57	8.3	0.189
5	3	Sec Trefoil	0.73	3.1	0.233
6	2	Ter Astigmatism	0.45		
7	1	Ter Coma	0.38		
5	5	Pentafoil	0.55	2.5	0.217
6	4	Sec Tetrafoil	0.56		

Figure 19: Estimated PM/SM Thermal WFE.

6. FINAL PEFORMANCE ERROR BUDGET

The initial error budget (Figure 6) assumed a simple uniform distribution of high-order contrast leakage. But, because some Zernike terms are more likely to occur than other terms, it is permissible to reallocate contrast leakage from the less likely terms to the more likely terms. Figure 20 shows an optimized error budget for the VVC-6 where the majority of the contrast leakage is allocated to trefoil. The first three data columns input the predicted STOP performance for each error source with its MUF (4X on LOS Jitter and LOS wavefront stability, 2X on inertial WFE stability and 3X on thermal WFE stability). These are RSSed to yield a total RMS WFE for each Zernike term. The VVC-6 Sensitivity column gives how many parts-per-trillion of Raw Contrast error leaks through the VVC-6 coronagraph for a pico-meter of Zernike WFE. The Raw Contrast column gives the predicted leakage for the STOP predicted Zernike WFE. The Allocation column normalizes and redistributes the 30 ppt of allowed raw contrast to maximize the amount allocated to Trefoil. The WFE Tolerance column is the new error budget. This error budget provides a margin of 4.1X for all Zernike. Please note that this error budget is ONLY for the baseline Zerodur primary mirror. A different mirror substrate or mount design will require a different error budget. And, the error budget will need to be adjusted for the 'as-built' mirror. Also, active WFE control via the ZWFS may add margin.

Index			Predicted Performance Amplitude [pm rms]			Total WFE	VVC-6 Sensitivity	Raw Contrast	Allocation	WFE Tolerance	Margin
N	M	Aberration	LOS	Inertial	Thermal	[pm rms]	[ppt/pm PV]	[ppt]	[ppt]	[pm RMS]	
		TOTAL RMS	5.715	3.994	5.565	8.921		7.289	30.000	36.715	
1	1	Tilt	3.025	0.123	0.026	3.027	0.0002	0.001	0.005	12.459	4.1
2	0	Power (Defocus)	0.728	1.430	3.759	4.087	0.0003	0.002	0.010	16.821	4.1
2	2	Astigmatism	4.674	3.559	3.463	6.819	0.0002	0.003	0.013	28.066	4.1
3	1	Coma	1.064	0.099	0.345	1.123	0.0002	0.001	0.002	4.620	4.1
4	0	Spherical	0.005	0.213	0.405	0.458	0.0003	0.000	0.001	1.883	4.1
3	3	Trefoil	0.050	1.039	2.098	2.342	1.0016	6.634	27.303	9.638	4.1
4	2	Sec Astigmatism	0.019	0.178	0.108	0.209	1.6495	1.091	4.489	0.861	4.1
5	1	Sec Coma	0.003	0.026	0.105	0.108	1.6645	0.624	2.568	0.445	4.1
6	0	Sec Spherical	0.000	0.028	0.000	0.028	2.8902	0.214	0.881	0.115	4.1
4	4	Tetrafoil	0.001	0.198	0.189	0.274	0.9312	0.806	3.317	1.127	4.1
5	3	Sec Trefoil	0.000	0.112	0.233	0.259	1.8200	1.630	6.708	1.064	4.1
6	2	Ter Astigmatism	0.000	0.021	0.000	0.021	2.7219	0.214	0.880	0.086	4.1
7	1	Ter Coma	0.000	0.033	0.000	0.033	3.0608	0.404	1.663	0.136	4.1
5	5	Pentafoil	0.000	0.074	0.217	0.229	2.4409	1.939	7.979	0.944	4.1
6	4	Sec Tetrafoil	0.000	0.029	0.000	0.029	2.2050	0.239	0.985	0.119	4.1
7	3	Ter Trefoil	0.000	0.015	0.000	0.015	2.7946	0.168	0.690	0.062	4.1
6	6	Hexafoil	0.000	0.026	0.000	0.026	3.1667	0.308	1.268	0.107	4.1
7	5	Sec Pentafoil	0.000	0.015	0.000	0.015	3.0694	0.184	0.758	0.062	4.1
7	7	Septafoil	0.000	0.010	0.000	0.010	2.6510	0.106	0.436	0.041	4.1

Figure 20: Optimized Error Budget for VVC-6.

7. SUMMARY

The Habitable Exoplanet Observatory Mission (HabEx) will image and spectroscopically characterize planetary systems around nearby sun-like stars. Critical to achieving HabEx's science goals is a large, ultra-stable UV/Optical/Near-IR (UVOIR) telescope. The desired telescope is a 4-meter off-axis unobscured three-mirror-anastigmatic, diffraction limited at 400 nm with wavefront stability on the order of a few 10s of picometers. The baseline HabEx telescope specifications were derived using science-driven systems-engineering. Its design was accomplished using standard engineering practice. And, its design 'closes'. STOP modeling predicts that the telescope meets with margin its specified error budget allocations for Line of Sight Jitter, LOS Wavefront Error, Inertial WFE and Thermal WFE. Key to meeting these specifications is the choice to use micro-thrusters for pointing control instead of reaction wheels. The baseline observatory design fits with margin within the mass and volume constraints of the SLS Block-2 8.4-m fairing.

ACKNOWLEDGEMENTS

This paper is the work of the NASA MSFC HabEx Team and our JPL Collaborators. MSFC Team: Thomas Brooks, Jacqueline Davis, Michael Effinger, Brent Knight, Scott Smith, Mark Stahl; Willian Arnold (AI Solution); Mike Baysinger (ESSCA), Jay Garcia (ESSCA), Mary Caldwell Ron Hunt, Andrew Singleton, and Melissa Therrell (ESSA); Bijan Nemati (UAH); and interns Jonathan Gaskin (UNCC), Jonathan McCready (NCSU), and Hao Tang (UoMI). JPL Team: Keith Warfield, Gary Kuan, Velibor Cormarkovic, Scott Howe, Stefan Martin, Navtej Saini, Stuart Shaklan, Juan Villalvazo, and Team X.

REFERENCES

[1] Habitable Exoplanet Observatory Final Report, NASA, 23 Aug 2019; https://www.jpl.nasa.gov/habex/pdf/HabEx-Final-Report-Public-Release.pdf

[2] Stahl, H. Philip, "Overview of a telescope concept design for the Habitable-zone Exoplanet Direct Imaging Mission", Proc. SPIE 10398, UV/Optical/IR Space Telescopes and Instruments: Innovative Technologies and Concepts VIII, 1039806 (5 September 2017); doi: 10.1117/12.2275192;

[3] Stahl, H. Philip, "Overview and performance prediction of the baseline 4-meter telescope concept design for the habitable-zone exoplanet observatory", Proc. SPIE 10698, Space Telescopes and Instrumentation 2018: Optical, Infrared, and Millimeter Wave, 106980W (6 July 2018); doi: 10.1117/12.2315291;

[4] Stahl, H. Philip, Gary Kuan, William Arnold Sr., Michael Baysinger, Thomas Brooks, Velibor Cormarkovic, Jacqueline Davis, Jay Garcia, J. Brent Knight, Stefan Martin, Navtej Saini, Hao Tang, Juan Villalvazo, "Habitable-zone exoplanet observatory (HabEx) baseline 4-m telescope design and predicted performance," Proc. SPIE 11115, UV/Optical/IR Space Telescopes and Instruments: Innovative Technologies and Concepts IX, 111150U (9 September 2019);

[5] H. Philip Stahl, Gary Kuan, William Arnold, Mike Baysinger, Thomas Brooks, Jay Garcia, J. Brent Knight, "Habitable-zone observatory (HabEx) baseline 4-m telescope design and predicted performance," Proc. SPIE 11443, Space Telescopes and Instrumentation 2020: Optical, Infrared, and Millimeter Wave, 114433C (13 December 2020); https://doi.org/10.1117/12.2562879

[6] Krist, Trauger, Unwin and Traub, "End-to-end coronagraphic modeling including a low-order wavefront sensor", SPIE Vol. 8422, 844253, 2012; doi: 10.1117/12.927143

[7] Harvey, James E. and Christ Ftaclas, "Diffraction effects of telescopes secondary mirror spiders on various image-quality criteria", Applied Optics, Vol. 34, No. 28, pp-6337, 1 Oct 1995.

[8] Nemati, Bijan, H. Philip Stahl, Mark T. Stahl, and Garreth Ruane "HabEx Telescope WFE stability specification derived from coronagraph starlight leakage", Proc. SPIE 10743, Optical Modeling and Performance Predictions X, 107430G (17 September 2018); doi: 10.1117/12.2312662;

[9] Nemati, Bijan, H. Philip Stahl, Mark T. Stahl, Garreth Ruane, "Method for deriving optical telescope performance specifications for Earth-detecting coronagraphs," JATIS (in-process)

[10] Morgan, Rhonda H., et. al., "HabEx yield modeling with for systems engineering", SPIE 10398-3, 2017.

[11] NASA, Exo-C: Imaging Nearby Worlds, CL#15-1197, March 2015, https://exep.jpl.nasa.gov/stdt/Exo-C_Final_Report_for_Unlimited_Release_150323.pdf

[12] Brooks, Thomas E., Ron Eng, Tony Hull, H. Philip Stahl, "Modeling the Extremely Lightweight Zerodur Mirror (ELZM) thermal soak test", Proc. SPIE 10374, Optical Modeling and Performance Predictions IX, 103740E (6 September 2017); doi: 10.1117/12.2274084

[13] Shaklan, Green and Palacios, "TPFC Optical Surface Requirements", SPIE 626511-12, 2006.

[14] Shaklan & Green, "Reflectivity and optical surface height requirements in a coronagraph", Applied Optics, 2006

[15] Stahl, H. Philip, Randall C. Hopkins, Andrew Schnell, David Alan Smith, Angela Jackman, Keith R. Warfield, "Designing astrophysics missions for NASA's Space Launch System," J. Astron. Telesc. Instrum. Syst. 2(4), 041213 (2016), doi: 10.1117/1.JATIS.2.4.041213

[16] Arnold, William R, H. Phillip Stahl, "Influence of core and hexapod geometry, and local reinforcement on the performance of ultra lightweight ULE mirror," Proc. SPIE 10743, Optical Modeling and Performance Predictions X, 107430B (17 September 2018); doi: 10.1117/12.2326017

[17] Arnold, William R., H. Philip Stahl, "Design trade Study for a 4-meter off-axis primary mirror substrate and mount for the Habitable-zone Exoplanet Direct Imaging Mission", Proc. SPIE 10398, UV/Optical/IR Space Telescopes and Instruments, 1039808 (5 September 2017); doi: 10.1117/12.2275193

[18] Davis, Jacqueline M., Philip H. Stahl, William R. Arnold, W. Scott Smith, "HabEx primary mirror trade studies", Proc. SPIE 10371, Optomechanical Engineering 2017, 103710B (5 September 2017); doi: 10.1117/12.2274476

[19] Arnold, William R., Ryan M. Bevan and H. Philip Stahl, "Integration of mirror design with suspension system using NASA's new mirror modeling software", Proc. SPIE 8836, 2013, doi: 10.1117/12.2023512

[20] Arnold, William R., "Evolving design criteria for very large aperture space-based telescopes and their influence on the need for intergrated tools in the optimization process," Proc. SPIE 9573, Optomechanical Engineering 2015, 95730G (2 September 2015); doi: 10.1117/12.2188570

[21] Brooks, Thomas E., Ron Eng, H. Phillip Stahl, "Optothermal stability of large ULE and Zerodur mirrors," Proc. SPIE 10743, Optical Modeling and Performance Predictions X, 107430A (17 September 2018); doi: 10.1117/12.2321275

[22] Harris Corporation, "SpaceviewTM 50/65/70 Small Satellite Imaging Soluitions" Specification Data Sheet, harris.com, 2019.

[23] Harris Corporation, "SpaceviewTM 110 Satellite Imaging Solution" Specification Data Sheet, harris.com, 2019.

[24] Harris Corporation, "PTC Thermal System Design Review", NASA Marshall Space Flight Center Contract NNM15AA01C, AMTD II, 17 July 2018,

[25] Ziemer, et. al., "Colloid Micro-Newton Thrusters for Precision Attitude Control", CL#17-2067, April 2017.